Separation Science and Technology
Publication details, including instructions for authors and subscription information:
http://www.informaworld.com/smpp/title~content=t713708471

Reverse Osmosis in an Unstirred Batch System. I. A Mathematical Model of Phenomenon

Chen-Chong Lin[a]; Gow-Jen Tsai[a]
[a] DEPARTMENT OF CHEMICAL, ENGINEERING NATIONAL TAIWAN UNIVERSITY TAIPEI, TAIWAN, REPUBLIC OF CHINA

To cite this Article Lin, Chen-Chong and Tsai, Gow-Jen(1982) 'Reverse Osmosis in an Unstirred Batch System. I. A Mathematical Model of Phenomenon', Separation Science and Technology, 17: 5, 727 — 737
To link to this Article: DOI: 10.1080/01496398208068563
URL: http://dx.doi.org/10.1080/01496398208068563

SEPARATION SCIENCE AND TECHNOLOGY, 17(5), pp. 727-737, 1982

Reverse Osmosis in an Unstirred Batch System. I. A Mathematical Model of Phenomenon

CHEN-CHONG LIN and GOW-JEN TSAI

DEPARTMENT OF CHEMICAL ENGINEERING
NATIONAL TAIWAN UNIVERSITY
TAIPEI, TAIWAN, REPUBLIC OF CHINA

Abstract

A mathematical model based on a two-parameter mechanism for reverse osmosis in a unstirred batch system has been theoretically developed and analyzed numerically. The model consists of a convective salt flux across the membrane and a salt diffusion equation which contains a nonlinear convective term with a moving boundary and which is solved by a finite difference procedure. A computer-aided analysis of the proposed model was compared with the analytical results of the different models available in the literature. It is found that the model proposed is in better agreement with the experimental data obtained by many investigators in the past.

INTRODUCTION

There are three types of experimental systems available for studying reverse osmosis: continuous flow, stirred batch, and unstirred batch systems. The advantage of the unstirred batch system is based on its simple geometrical configuration and experimental facility. The study on this phenomenon was first dealt with by Raridon et al. (*1*) in which the two main features of constant rate and absence of mass transport downstream of the membrane were assumed. Astarita and Greco (*2*) improved on Raridon's model by taking into account the material transferred to the effluent stream. On the other hand, Liu and Williams (*3*) identified two different polarization regimes; the rejection loss and the diffusion wave. The main difference between them is that, in the rejection loss regime, the final value of the effluent flow rate which is reached at infinite time is not zero, while in the diffusion wave regime its asymptotic value is zero. Finally, Williams (*4*) gave a relationship to calculate the dimensionless interface salt concentration

upstream of the membrane. Alfani and Drioli (5) described the results of a mathematical model which takes into account the mass transport downstream of the membrane and the flow-rate dependency from the interfacial concentrations. Later, Alfani and Drioli (*6, 7*) made theoretical and experimental treatments for a semitheoretical solution of the problem which used empirical results. The purpose of this paper is to develop a new model which will be able to predict the transport phenomena in a reverse osmosis, unstirred batch system.

MODEL DEVELOPMENT

A dimensional unstirred batch reverse osmosis cell is schematically shown as Fig. 1. Use of an asterisk (*) by the symbols used always refers to the defined dimensional variables, while the subscripts (0) and (1) refer to positions upstream and downstream of the membrane, respectively. Before beginning a detailed discussion, it is useful to note that our model depends on a number of assumptions including

(1) Constancy of liquid density on each space point in the system at each time considered, i.e., $\rho \neq \rho(Z^*, \tau^*)$
(2) Validity of two parameter model of membrane transport mechanism, i.e.,

$$N_A^* = B(\rho_{A0} - \rho_{A1}) \tag{1}$$

$$N_B^* = A(\Delta P - \Delta\pi) \tag{2}$$

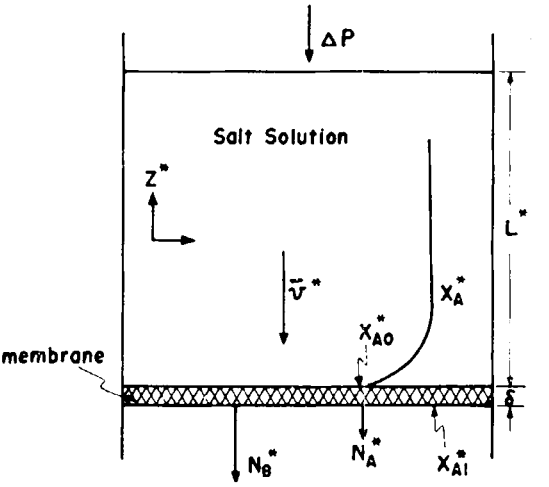

FIG. 1. Schematic representation of one-dimensional unstirred batch reverse osmosis cell.

(3) The membrane constants, A and B, are independent of salt concentration and time, i.e., A or $B \neq f(X_A^*, \tau^*)$
(4) Assuming the steady-state flows of solute and solvent across the membrane
(5) Neglecting the pressure drop caused by the liquid level, i.e., $\Delta P \gg \rho g L^*$, where g is gravity
(6) Constancy of the diffusion coefficient at different salt concentrations, i.e., $D_{AB} \neq f(X_A^*)$
(7) Neglecting viscous flow along the cell wall

Owing to the intrinsic salt rejection effect of the membrane, the salt concentration near the membrane surface will increase with elapsed time. As a consequence, the salt rejection efficiency of the membrane progressively decreases, resulting in a moving boundary of the system which is known as the variable rejection model. Assuming that only convective and diffusive material transfer occur and neglecting viscous flow along the wall, the differential material mass balance equation for solute becomes

$$\frac{\partial X_A^*}{\partial \tau^*} + \bar{v}^* \frac{\partial X_A^*}{\partial Z^*} = D_{AB} \frac{\partial^2 X_A^*}{\partial Z^{*2}} \tag{3}$$

The following represent the initial and boundary conditions to which Eq. (3) is subjected:

Initial condition:

$$\text{at } 0 \leq Z^* < L^{*0}, \qquad \tau^* = 0, X_A^* = X_A^{*0}$$

Boundary conditions:

$$(1) \text{ at } Z^* = 0, \qquad N_A^* = \rho_A \bar{v}_A^*$$

$$= \rho \left(X_A^* \bar{v}^* - D_{AB} \frac{\partial X_A^*}{\partial Z^*} \right)$$

$$(2) \text{ at } Z^* = L^*, \qquad \partial X_A^* / \partial Z^* = 0$$

The superscript (0) by the symbols refers to the initial or feed stage. Now,

$$\bar{v}^* = \frac{dL^*}{d\tau^*} = \frac{1}{\rho}(N_A^* + N_B^*) \tag{4}$$

where N_A^* and N_B^* can be substituted from Eqs. (1) and (2), respectively. They become

$$N_B^* = A(\Delta P - \Delta \pi)$$

$$= A\{\Delta P - [\pi(X_{A0}^*) - \pi(X_{A1}^*)]\}$$

where the values of $\pi(X_A^*)$ can be approximated by the following equation if the solution is not dilute enough to make use of the Van't Hoff equation:

$$\pi(X_A^*) = a + bX_A^* + cX_A^{*2} + dX_A^{*3} + eX_A^{*4} \tag{5}$$

where a, b, c, d, and e are constants.

The following relation is also valid according to Assumption (4):

$$X_{A1}^* = \frac{N_A^*}{N_A^* + N_B^*} \tag{6}$$

Upon the choice of suitable dimensionless variables as listed in Table 1, Eqs. (3), (4), and (6) result in

$$\frac{\partial X_A}{\partial \tau} + V\frac{\partial X_A}{\partial Z} = \frac{\partial^2 X_A}{\partial Z^2} \tag{7}$$

$$V = dL/d\tau = N_A + N_B \tag{8}$$

$$N_A = E(X_{A0} - X_{A1})$$

$$N_B = F(1 - G(X_{A0} - X_{A1}) - H(X_{A0}^2 - X_{A1}^2) - I(X_{A0}^3 - X_{A1}^3) - J(X_{A0}^4 - X_{A1}^4)$$

$$X_{A1} = \frac{1}{X_A^0}\,\frac{N_A}{N_A + N_B} \tag{9}$$

TABLE 1

Dimensionless Variables

$$\tau = \frac{D_{AB}\tau^*}{(L^{*0})^2}, \quad Z = \frac{Z^*}{L^{*0}}, \quad X_A = \frac{X_A^*}{X_A^{*0}}, \quad L = \frac{L^*}{L^{*0}}$$

$$V = \frac{\bar{v}^* L^{*0}}{D_{AB}}, \quad N_A = \frac{N_A^* L^{*0}}{\rho D_{AB}}, \quad N_B = \frac{N_B^* L^{*0}}{\rho D_{AB}}$$

$$E = \frac{BL^{*0}X_A^0}{D_{AB}}, \quad F = \frac{AL^*\Delta P}{\rho D_{AB}}, \quad G = \frac{bX_A^0}{\Delta P}$$

$$H = \frac{C(X_A^0)^2}{\Delta P}, \quad I = \frac{d(X_A^0)^3}{\Delta P}, \quad J = \frac{e(X_A^0)^4}{\Delta P}$$

The initial and boundary conditions for these dimensionless equations are now as follows:

Initial condition:

$$\text{at } 0 \leq Z \leq 1, \qquad \tau = 0,\ X_A = 1.0$$

Boundary conditions:

$$(1)\ \text{at } Z = 0,\ \tau > 0, \qquad N_A = X_A^0 \left(X_A V - \frac{\partial X_A}{\partial Z} \right)$$

$$(2)\ \text{at } Z = L, \qquad \tau > 0,\ \partial X_A / \partial Z = 0$$

Differential equation (7) with the pertinent boundary conditions mentioned was solved numerically by a finite differential procedure in conjunction with an iteration method. An immobilized axis is employed in order to facilitate the solution which minimizes the computation time required. These techniques and computer program are discussed more fully in Ref. *8*.

RESULTS AND DISCUSSION

The desalination capacity of a membrane may be expressed in several ways. The most commonly used term is the percent salt rejected, $\%SR$, defined as

$$\%SR = \left(\frac{\rho_{A0} - \rho_{A1}}{\rho_{A0}} \right) \times 100 \tag{10}$$

Under the conditions of $N_A^* \ll N_B^*$ and $\rho_{H_2O} \simeq \rho$, this can be approximated by the two-parameter model as

$$\%SR = \left[1 + \frac{\rho B}{A(\Delta P - \Delta \pi)} \right]^{-1} \times 100 \tag{11}$$

It is evident that $\%SR$ is a function of $(\Delta P - \Delta \pi)$, which is a function of time. Although Alfani's model (*6*) took into account the flow rate dependency on the interface concentration which was based on experimental data, the differential mass balance equation could be only solved semi-theoretically. Namely, it cannot be used to predict the polarization phenomenon since it needs the aid of experimental data in order to evaluate the salt concentration profiles. Figure 2 shows the time dependence of the dimensionless flow rate. The numerical values used in our model and some analytical results corresponding to theory are listed in Table 2. The amount of information generated are discussed as follows.

Considering the $\%(SR)^0$ to be 99 and 97%, then all models are analyzed to

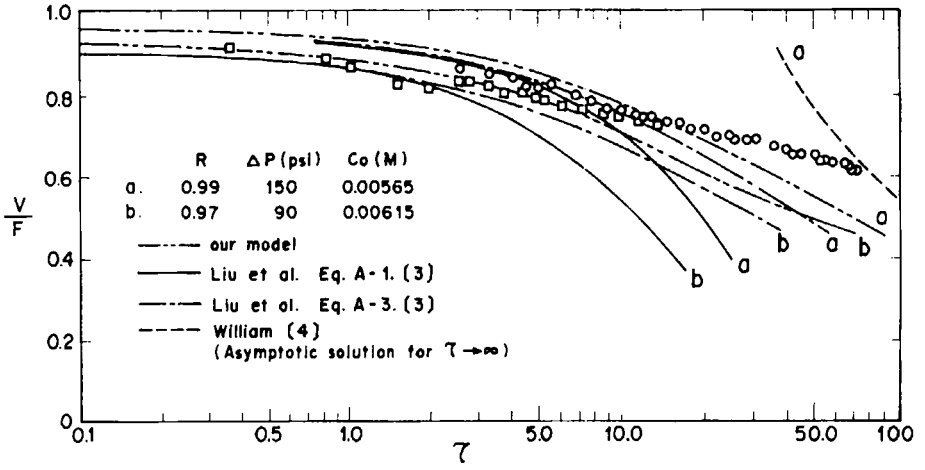

FIG. 2. Time dependence of flow rate in unstirred batch reverse osmosis cell. (□, ○) Experimental data from Liu and Williams [3].

obtain the curves as plotted in Fig. 2, showing that all curves appear to agree with experimental data at the lower τ stage. However, at larger τ all models tend to deviate from the experimental data. For instance, when $\tau = 50$, curve a differs from the experimental data by about 25% for both integral and asymptotic methods, while by only 12% for our model, which lies closest to the experimental data. One will realize from Table 2 that $\%SR$ cannot be kept unchanged during the time of operation. It changes, for instance, from 99% to 97.95% at τ goes from zero to 80.68 under Condition (a).

TABLE 2

Summary of Effect of Simulation Parameters on Some Analytical Results

	$A\left(\frac{\text{g}}{\text{cm}^2\cdot\text{s}\cdot\text{atm}}\right)$	B (cm/s)	$\%(SR)^0$	$\%SR(\tau)$	$X_{A0}(\tau)$	$X_{A1}(\tau)$
Fig. 2, a[a]	1.65×10^{-5}	1.46×10^{-6}	99.01	97.95	20.47	0.419
Fig. 2, b[a]	1.47×10^{-5}	2.57×10^{-6}	97.09	93.90	12.36	0.754
Fig. 3, a[b]	1.95×10^{-5}	8.50×10^{-6}	89.16	81.40	5.46	1.01
Fig. 3, b[b]	1.95×10^{-5}	7.50×10^{-6}	90.30	82.38	5.72	1.00

[a] $\tau = 80.68$, π is calculated by the Van't Hoff equation.
[b] $\tau = 125.6$, π is calcualted by Eq. (5).

Experimental data of a log-log plot of the throughput rate vs time (dimension) by Alfani et al [7] under a pressure of 4 atm showed a rejection loss regime behavior as shown in Fig. 3. Our model using $D_{AB} = 2.257 \times 10^{-5}$ cm^2/s (*9*) shows the same feature as the experimental curve (see Curves a and b of Fig. 3). As $\tau^* \to \infty$, the accuracies are about 14 and 8% for Curves a and b, respectively. A rather large discrepancy (~20%) has been observed in the intermittent time, i.e., at 10 h $\leq \tau^* \leq$ 40 h, indicating the overestimation of the flow rate due to Assumption (4) during this intermittent time.

The experimental salt concentration of effluent is plotted vs time as shown in Curve 1 of Fig. 4. The curves obtained by the analytical solution of the constant rejection models proposed by Raridon (*1*), Astarita (*2*), and Alfani et al. (*5*), and a semiempirical variable rejection model by Alfani et al. (*7*) are graphically compared by the solid Curves 6, 5, 4, and 3, respectively. Curve 2 is the simulation result.

The V shape of the experimental curve (Curve 1) is probably due to the experimental error caused by an improper probe for X_{A1} on which Alfani's model (Curve 3) was based. At small τ, the data are more sensitive to the inadequate probe. When $\tau > 15$, the influence is assuaged and the experimental concentration data for X_{A1} fit fairly well with the curve calculated from our model.

By a comparison of the plots of the interface salt concentration upstream of the membrane, X_{A0}, vs time as shown in Fig. 5, the curve of our model fits

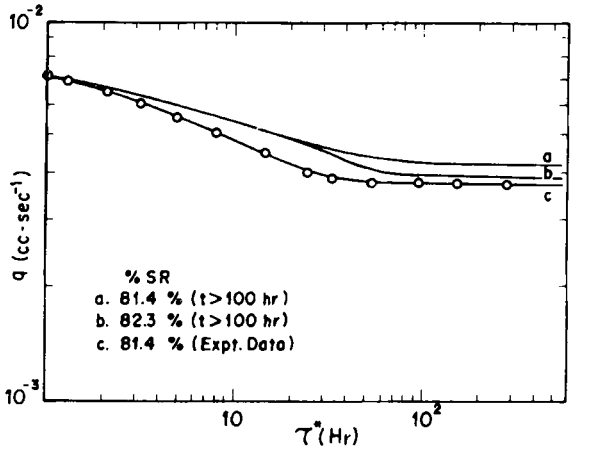

FIG. 3. Predicted log-log diagram of NaCl solution flow rate vs time. $\Delta P = 4.0$ atm, $C^0 = 0.0109$ *M*, $T = 40$°C. (○) Experimental data from Alfani et al. [7]. Curves a and b are from our model.

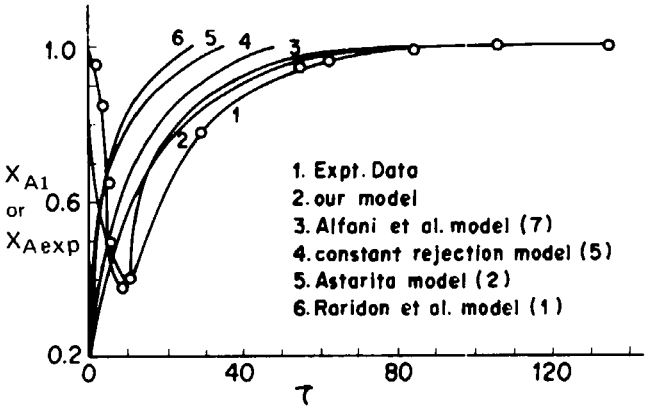

FIG. 4. Plots of experimental effluent NaCl concentration (Curve 1) and predicted interface NaCl concentration downstream of the membrane vs time. $\Delta P = 4.0$ atm, $C^0 = 0.0109$ M, temperature = 40°C. (○) Experimental data from Alfani et al. [7].

best with the experimental data measured by Alfani et al. (7). Finally, $\%SR$ vs time is plotted in Fig. 6 using the same experimental conditions as described in Figs. 3, 4, and 5. Our model shows a progressive change in $\%SR$ from 89.16 to an asymptotic value of 81.4%, while the semiempirical model shows a sudden change from zero to an asymptotic constant value. Curve b of

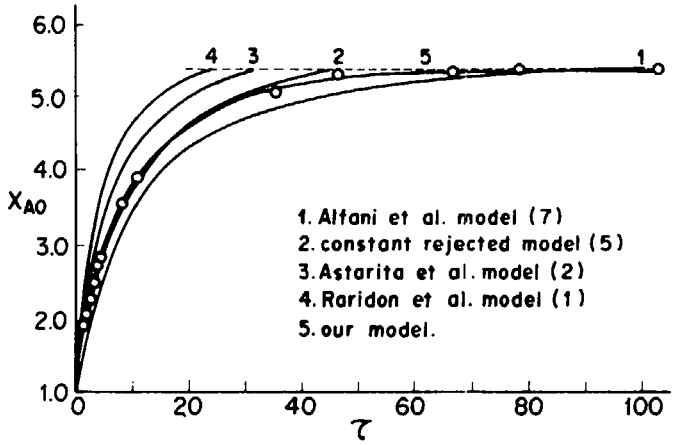

FIG. 5. Predicted plot of the interface NaCl concentration upstream of the membrance vs time. $\Delta P = 4.0$ atm, $C^0 = 0.0109$ M, temperature = 40°C. (○) Experimental data from Alfani et al [7].

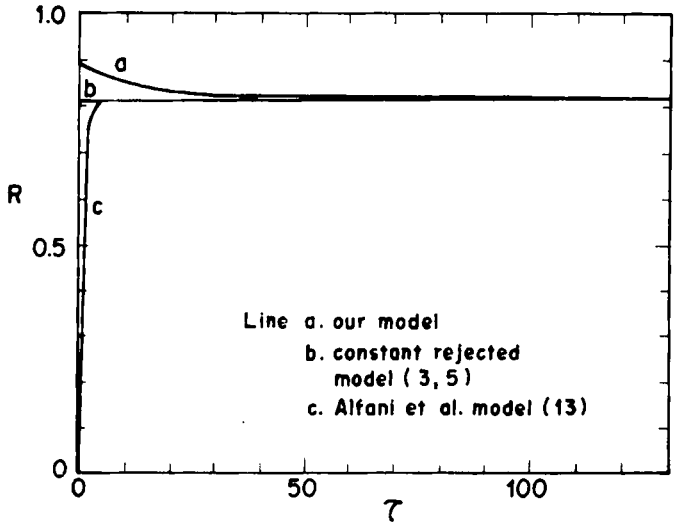

FIG. 6. Plot of predicted salt rejection vs time.

Fig. 6 represents a constant rejection model. It is apparent our model describes the most reasonable feature of a variable rejection. A method to evaluate the aptness of the model was proposed by Alfani et al. (7), based on the fact that the salt accumulation in the upper cell also coincides with the overall salt loss of the solution across the membrane:

$$\int_0^\infty A(X_A - 1)\, dZ^* = \int_0^\infty q(1 - X_{A0})\, d\tau^* \tag{12}$$

and

$$\int_0^\infty q(1 - X_{A0})\, d\tau^* = \int_0^\infty q(1 - X_{A0/\text{exp}})\, d\tau^* \tag{13}$$

Performing the numerical calculations and setting the value of the right side of Eq. (13) equal to 1, the left side of Eq. (13) computed for Curves 1, 2, 3, 4, and 5 in Fig. 5 are worth 0.923, 0.677, 0.486, 0.386, and 1.05, respectively. This result appears to prove that our model is the most apt to describe the concentration phenomena in such an unstirred batch cell for reverse osmosis.

SYMBOLS

A a membrane constant ($g/cm^2 \cdot s \cdot atm$), surface area of membrane (cm^2)

B	a membrane constant (cm/s)
C	concentration of liquid (mol/L)
D_{AB}	diffusion coefficient of solute (cm^2/s)
L^*	liquid level (cm)
N^*	effluent flux through the membrane ($g/cm^2 \cdot s$)
ΔP	hydrostatic pressure difference across the membrane (atm)
q	throughput rate (cm^3/s)
R	salt rejection
$\%SR$	percent salt rejected
$\bar{v}^*$	average velocity (cm/s)
X^*	weight fraction
Z^*	axial dimension (cm)

Superscripts

*	dimensional quantity
0	initial or at feed

Subscripts

A	salt solute
B	water solvent
0	upstream of the membrane
1	downstream of the membrane

Greek

δ	thickness of membrane (cm)
$\Delta\pi$	difference between the osmotic pressure of salt solution and that of the effluent (atm)
τ^*	time (s)
ρ	mass concentration (g/cm^3), density of liquid (g/cm^3)

REFERENCES

1. R. J. Raridon, L. Dresdner, and K. A. Kraus, *Desalination*, *1*, 210 (1966).
2. G. Astarita and G. Greco, Jr., *Chim. Ind.*, *52*, 49 (1970).
3. M. K. Liu and F. A. Williams, *Int. J. Heat Mass Transfer*, *13*, 144 (1970).
4. F. A. Williams, *Siam J. Appl. Math.*, *17*, 59 (1969).
5. F. Alfani and E. Drioli, *Ing. Chim., It.*, *8*, 235 (1972).
6. E. Drioli, F. Alfani, and G. Iorio, *Chim. Ind.*, *53*, 674 (1971).
7. F. Alfani and E. Drioli, *Chem. Eng. Sci.*, *29*, 2197 (1974).

8. G. J. Tsai, MS Thesis, National Taiwan University, 1979.
9. R. H. Perry and C. H. Chilton, *Chemical Engineers' Handbook*, 5th ed., McGraw-Hill, New York, 1973, pp. 3-235.

Received by editor July 17, 1981